Schweizerische Eidgenossenschaft
Confédération suisse
Confederazione Svizzera
Confederaziun svizra

Eidgenössisches Departement für
Umwelt, Verkehr, Energie und Kommunikation UVEK

Office fédéral de l'énergie OFEN

SOLAIR

INNOVATIVE SOLAR COLLECTORS FOR EFFICIENT AND COST-EFFECTIVE SOLAR THERMAL POWER GENERATION

Rapport Final

Auteur et coauteurs	M.C. Barbato, Ph. Haueter, R. Bader, A. Steinfeld, A. Pedretti
Institution mandatée	ALE Airlight Energy SA
Adresse	Via Croce, 1 Biasca – CH-6710
Téléphone, e-mail, site Internet	+41 91 873 0505
N° projet / n° contrat OFEN	102327
Responsable OFEN du projet	
Durée prévue du projet (de - à)	01-12-2007 --- 31-12-2008
Date	30/12/2008

RÉSUMÉ

This report presents the main results of the project. The project has been started at the end of 2007 and has been successfully finished in December 2008.

The present project of ALE AirLight Energy aims at the engineering investigation and design of a novel concept of a solar collector system for efficient and cost-effective solar thermal power generation. The technology exploits an air-inflated reflective structure for concentrating solar radiation. This new arrangement reduces investment costs of the collector field and promises to be economic competitive. A first prototype, built in 2007, has been re-designed and heavily modified during this project. In the new configuration, by using secondary mirrors, the focal area is located close to the main structure and allows the integration of the receiver in the inflated structure.

The topics expanded in this document are as follows:

- Design solutions for the concentrated energy receiver suitable for the revised SolAir concentrator concept.
- Solar flux simulation via Monte Carlo method.
- New version of the ALE AirLight Energy concentrator prototype.
- Prototype radiative flux measurements.

Buts du projet

The present project aims at the engineering investigation and design of a breakthrough concept of a solar collector system for efficient and cost-effective solar thermal power generation. The novel collector technology exploits a revolutionary air-inflated reflective structure for concentrating solar radiation. Since this new arrangement reduces drastically the investment costs of the collector field, the solar thermal plant promises to be highly economic competitive.

Travaux effectués et résultats acquis

1 – RECEIVER DESIGN (SUPSI)

The receiver is the component that has the role of converting the concentrated electromagnetic solar energy into thermal energy and to transmit this energy to a working fluid that act as thermal energy carrier.

For the SolAir project, the first receiver design concept, that is shown in Figure 7 and has been presented in the 2007 Project Report [1], has been changed following the idea of using a different working fluid.

At the initial stage of the project, the selected working fluid was a liquid, either water or oil. Further studies and analyses of the specific features of the SolAir concentrator new design, lead to explore the possibility to use a gaseous energy carrier.

Therefore in this part of the project SUPSI performed a detailed study to design a receiver with a gaseous working fluid and to predict its performance.

The receiver design solutions explored can be summarized in two families:

- tubular receivers;
- cylindrical cavity receivers.

Besides the obvious technical needs to be fulfilled (among those, we have to remember that the concentrator mirror is cylindrical and this makes the concentrated solar energy focus to be a plane) two major issues have driven the receiver design: simplicity and low cost, two factors that are among the main driving forces of the SolAir collector project.

1.1 – Receiver Study

For each receiver model of the two families, a series of thermo fluid dynamic simulations have been performed to verify the receiver efficacy and to evaluate, as a first approximation, the performances in terms of energy transmission to the working fluid and flow pressure drop. In fact, energy transmission efficiency is relevant for the whole collector efficiency, whereas the flow pressure drop is an important issue directly linked to the pumping power needed for running the collectors plant. The latter issue has major importance when using a gaseous energy carrier with respect to the case of a liquid working fluid. In fact, large masses of fluid have to be pumped and, being the pumping work directly dependent on the fluid specific volume:

$$l = -\int_1^2 v\, dp$$

(where v is the specific volume, p is the pressure and l is work for unit mass of fluid, for a reversible transformation with small changes of potential and kinetic energy) it appears evident how, keeping low the pressure losses is of paramount importance for keeping low the pumping power costs and avoid to excessively reduce the overall solar plant efficiency.

1.1.1 – Tubular Receivers

Tubular receivers have been designed creating a target region on cylindrical pipes. For these receivers, that can be classified as *external receivers* [3], the target region is a flat part of the tube (a stripe) that is hit by the solar radiation concentrated by the cylindrical mirrors (a schematic of the cross section is shown in Figure 1). The gaseous fluid flows inside the tube and exchanges thermal energy with the hot target. A thick layer of insulating material covers the part of the tube that is not exposed to the concentrated beam. A series of devices have been tested to enhance the energy transfer from the target stripe to the fluid. Dimensional details of cross sections of receivers using these devices are reported in Annex A. Some images with simulations results for these receivers can be seen in Figure 8 - Figure 11.

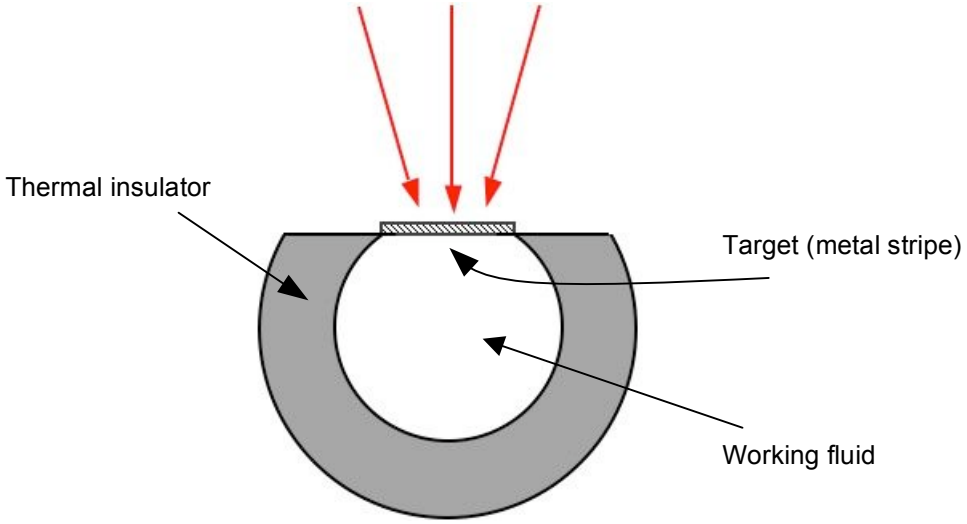

FIGURE 1: TUBULAR RECEIVER (CROSS SECTION).

1.1.2 – Cylindrical Cavity Receivers

Cylindrical cavity receivers design has been instead based on the concept of capturing the radiation in an insulated enclosure with an aperture that just allows the inlet of the concentrated radiation beam (Figure 2). The target surface inside the enclosure has a much larger area whit respect to the tubular receivers concept presented above. The working fluid flows axially in the annulus and extracts the energy from the cavity walls. The concentrated radiation focus is located at the cavity entrance and the radiation that reaches the inner target surface is defocused to some extent. The interior of the cavity is painted with a black coating. No special coatings are required because the emittance of this coating is not critical for thermal losses. In fact, for this receiver what is relevant is the dimension of the aperture: the opening has effective emittance almost unity because of its size with respect to the cavity size [4]. However, Bader in [2] has shown that the cavity optical efficiency depends both on the aperture dimension and on the inner wall absorptances with maximum values that are shifted toward larger apertures dimensions at higher wall absorptances. The existence of an optimal aperture dimension is therefore foreseen.

In the literature [4], [6] is reported that one of the advantages of the cylindrical cavity receiver with respect to tubular receivers is the relatively low flux density of adsorbed radiation. This fact allows for a different distribution of the incoming energy, which leads to lower and more distributed flux density of adsorbed radiation. This avoids that limited parts of the receiver tube reach very high temperatures generating also large temperature gradients inside the metal. This condition is particularly favorable to thermal losses when the fluid flow shows a low heat transfer coefficient. In fact, the larger is the temperature difference between metal and fluid, the larger are the thermal losses and higher are the values of generated entropy. Bader in [2] has performed a study on the energy flux density distribution on the cavity walls from the optical point of view. The interesting results of this study, which show instead a not really uniform flux density distribution (see Figure 3), will be used as input data for the future

thermo fluid dynamics simulations that will allow a deeper analysis of the receiver expected performances.

Also for this family of receivers, the duct parts that are not struck by the concentrated solar radiation are insulated with a thick layer of insulating, low cost material to reduce convective and radiative heat losses. Furthermore, the insulator “v” shape at the receiver opening is an important feature for reducing thermal radiation losses. In fact, the surfaces of the v-shaped insulation layer create a reduction of the optically opened environment surrounding the cavity aperture which, in this way, becomes much less than a 180° half plane (see Figure 2). The part of thermal energy irradiated through the cavity aperture to the insulator v-shaped walls is reradiated in a diffuse manner several times causing a reduction of the amount of thermal radiative losses from the aperture. The amount of this reduction depends on the angle of the v-shaped walls [4].

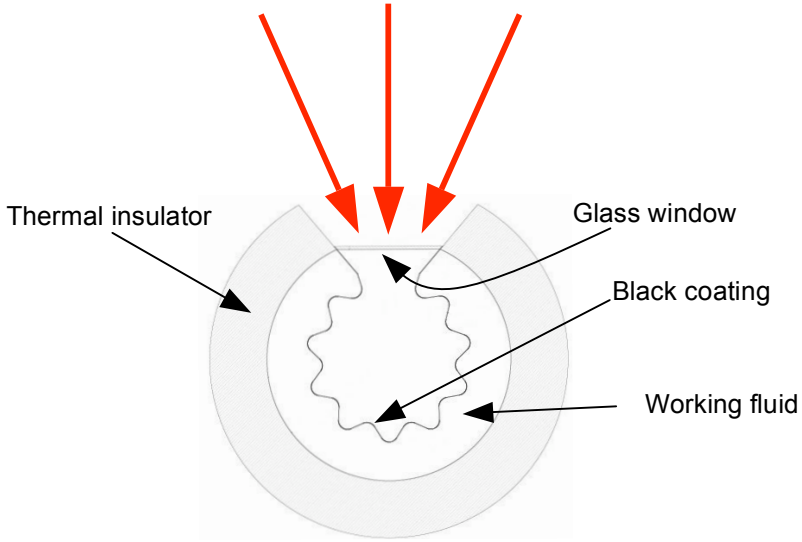

FIGURE 2: CYLINDRICAL CAVITY RECEIVER (CROSS SECTION).

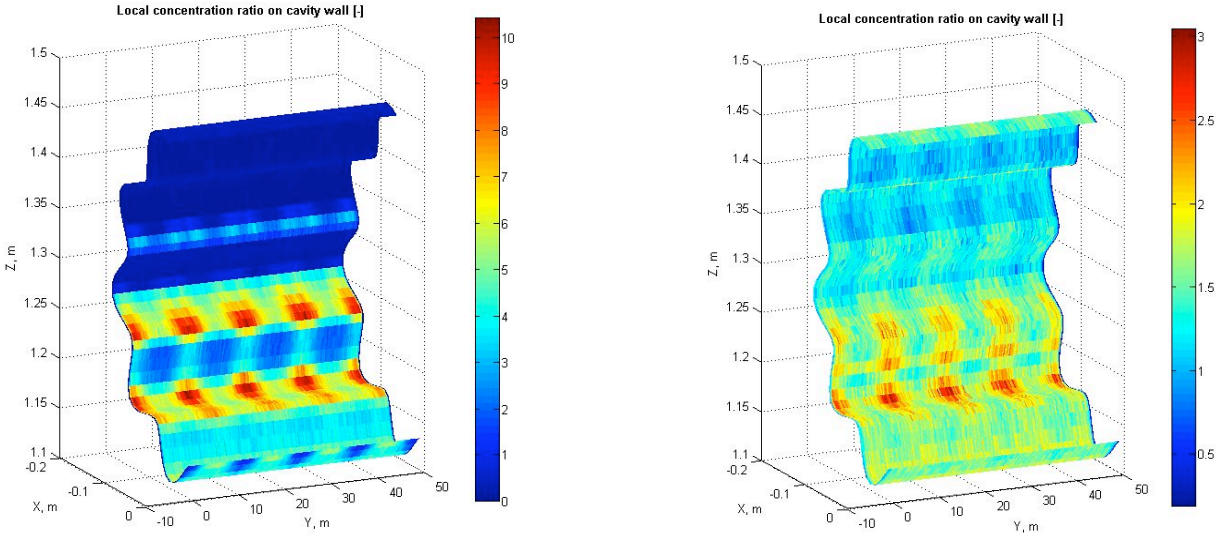

FIGURE 3: LOCAL CONCENTRATION RATIO ON THE CAVITY WALLS FOR DIFFERENT VALUES OF ABSORPTANCES (0.9 ON THE LEFT HAND SIDE; 0.1 ON THE RIGHT HNAD SIDE). THE RATIO OF SPECULAR TO TOTAL REFLECTANCE IS 0.4 IN BOTH CASES. FIGURES FROM [2].

1.1.3 – Receivers position

A big advantage of the new SolAir collector concept is that the receiver is located inside the ETFE cushion as it is shown by FIGURE 4. This protects the receiver from the wind reducing, as a consequence, the convective heat losses.

Another benefit offered by this configuration comes from the possibility of inflating the collector cushion with N_2 leading to a non oxidizing atmosphere for the receiver.

The new receiver position has been achieved by using secondary mirrors that allowed shortening the focus distance from the primary mirrors (see Figure 6). A known consequence of the usage of secondary mirrors is a small reduction of the collector optical efficiency (a schematic description of this can be found in Figure 5). We have to notice that this loss of efficiency is lower with respect to that caused by the passage of the concentrated radiation trough the ETFE as it was necessary in the first prototype design which had the receiver located outside of the ETFE cushion (see FIGURE 20).

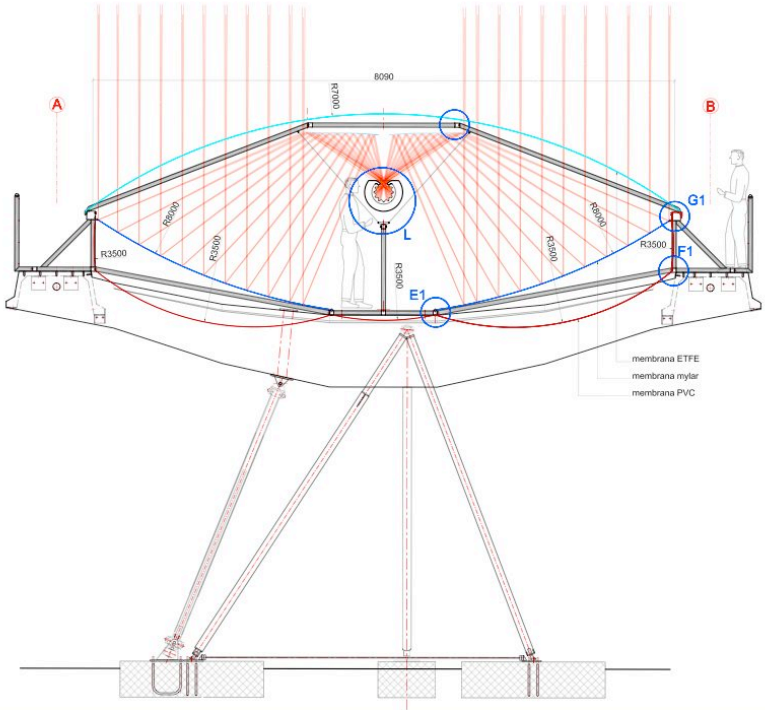

FIGURE 4: NEW PROTOTYPE SOLAR COLLECTOR – CROSS SECTION (SHOWN DIMENSIONS ARE IN MILLIMETERS).

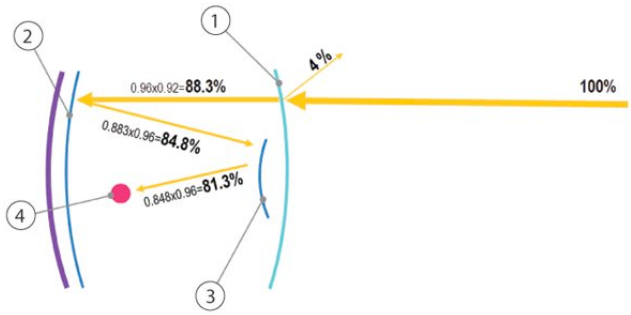

FIGURE 5: SCHEMATIC OF OPTICAL EFFICIENCIES VALUES FOR THE DOUBLE MIRROR SYSTEM.

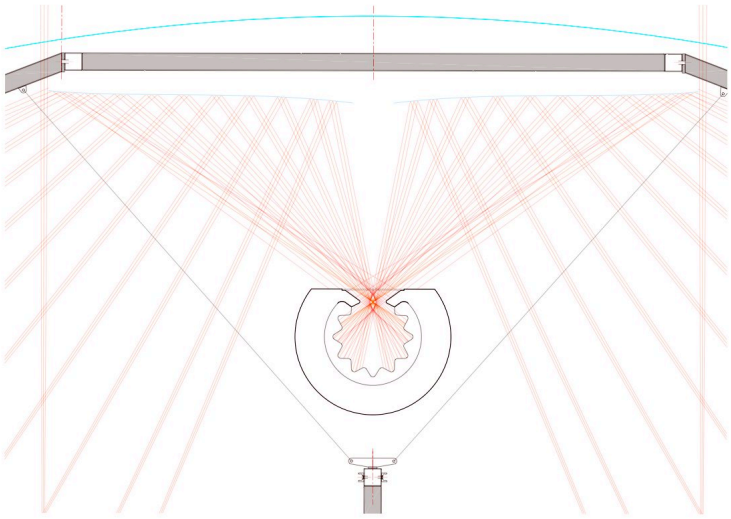

FIGURE 6: NEW PROTOTYPE SOLAR COLLECTOR – PARTICULAR: DEVIATION OF RAYS COMING FROM PRIMARY MIRRORS OBTAINED BY USING SECONDARY MIRRORS. THESE MIRRORS ARE ALSO LOCATED INSIDE THE ETFE CUSHION.

1.1.4 – Working Fluid

The working fluids considered for the new receiver design are Air and Nitrogen. There are several reasons for this choice:

- Air and N_2 are low cost working fluids (even no cost for air, made exception for the pumping power);
- Air and N_2 are not polluting, non aging fluids (no costs of replacement);
- Air can offer feasible solutions for energy storage (this is a topic to be studied in detail for the pilot SolAir Plant);
- these working fluids choice is coherent with the project philosophy of “keeping the system simple and low cost”.

On the other hand, Air and N_2, as energy carriers, are less effective than water and oil; they have lower densities and lower specific heats, which leads to much lower thermal capacities. Furthermore, Air and N_2 flows have much lower Reynolds numbers, which means also much lower heat exchange coefficients.

When using these working fluids, their mass flow rate has to be relatively large leading to high flow velocities and to pressure losses that can play an important role in the energetic efficiency of the collector. For this reason, receiver flow pressure drops are one of the most important parameters that have been monitored in the simulations performed at SUPSI.

1.1.5 – Simulations Details

The thermo-fluid dynamics simulations have been performed using the software package Fluent distributed by Ansys ltd. The model used in this work solves the Navier-Stokes equations in their time averaged form suitable for turbulent flows. Turbulence is modeled by using the “Realizable kε” two equations model [7]. Buoyancy effects are accounted for as well as the coupling of fluid and solid heat transfer (conjugate heat transfer model, i.e., convective plus conductive heat transfer). The boundary conditions used for solid walls are *enhanced wall functions* [8].

Some hypotheses have been done to balance accuracy and complexity of the model. Among those we can list:

- only a segment of the 250 m long receiver has been simulated.

- the electromagnetic radiation concentrated by the mirrors has been assumed to be uniformly distributed on the target surfaces, both for the tubular and for the cylindrical cavity receivers.
- convective losses for the glass external face and for the outer insulating material surface have been neglected.

The mass flow rate of working fluid has been evaluated starting from the design data available. Considering a 250 m long receiver and inlet and outlet temperatures as known we can write for the thermal power extracted by the fluid:

$$\dot{W} = \dot{m} c_p (T_{out} - T_{in})$$

where $\dot{m}$ is the mass flow rate, c_p is the specific heat, T_{in} the fluid inlet temperature and T_{out} the fluid outlet temperature. This thermal power is only part of the incident electromagnetic power. The efficiency of this extraction is defined by the coefficient [5]:

$$\gamma = \frac{\dot{m} c_p (T_{out} - T_{in})}{I_D S}$$

where, with the incident radiation I_D = 1000 W/m^2 and the mirror surface S = 250 x 10 m^2 (for a 250 m long collector with a 10 m wide primary mirror).

For the CFD simulations a conservative value of this efficiency ranging from 0.5 to 0.6 has been assumed and the working fluid mass flow rate has been calculated assuming for the fluid an outlet temperature of 550°C and a inlet temperature of 120°C. The calculated values are reported in Table 1.

All simulations have been performed on a cluster of Linux machines equipped with AMD double or quad core processors.

1.1.6 – Simulations Main Results

The simulations have shown that performances obtained with the tubular receivers are very poor for the air flow conditions required by the SolAir collector (see Table 1). The systems with finned targets are not very efficient for the transfer of thermal energy to the fluid. The hot part of the fins is small and flow passing through the fins is very slow compared to the main flow velocity (see Figure 8 and Figure 9). Special fins designs have also been tested to overcome these problems, but no meaningful enhancements have been obtained. Poor thermal performances have been obtained also changing the fins material looking for metals with high thermal conductivity (e.g. copper) as done by other authors for different receiver geometries [6]. Another problem found using finned target is the particularly high flow pressure drop, that would imply excessive costs in terms of pumping energy.

The cylindrical cavity receivers instead are those that performed better. Several geometries have been tested together with different operative pressures (from atmospheric up to 8 bar absolute pressure). Besides Air also Nitrogen and Water Vapor have been tested as working fluids for these second family of receivers. Some of the CFD results are shown in Figure 12- Figure 13 whereas Table 1 shows a summary of the relevant quantitative results.

The simulations have shown that the cylindrical cavity receiver concept works properly and that the receiver transforms and transfers the concentrated electromagnetic energy into working fluid thermal energy. The issue that now appears as the most critical is that of flow pressure losses. In fact, large masses of fluid have to flow at relatively high velocities into very long receivers and connecting pipes. This implies that the pumping power to involve is relevant. Therefore the pressure losses reduction is a primary target, but is also a controversial one. In fact, a possible solution to this issue will drive towards a reduction of the working fluid flow velocity, but this will affect negatively the effectiveness of the convective heat exchange. Testing of different receivers designs is devoted to find answer issues like this one and the thermo-fluid dynamics simulation model assessed up to now has been and will continue to be a useful tool for this kind of analyses. We have to notice, nevertheless, that the thermo-fluid dynamics simulation model will increase its efficacy once a validation against a prototype of the real system will be performed.

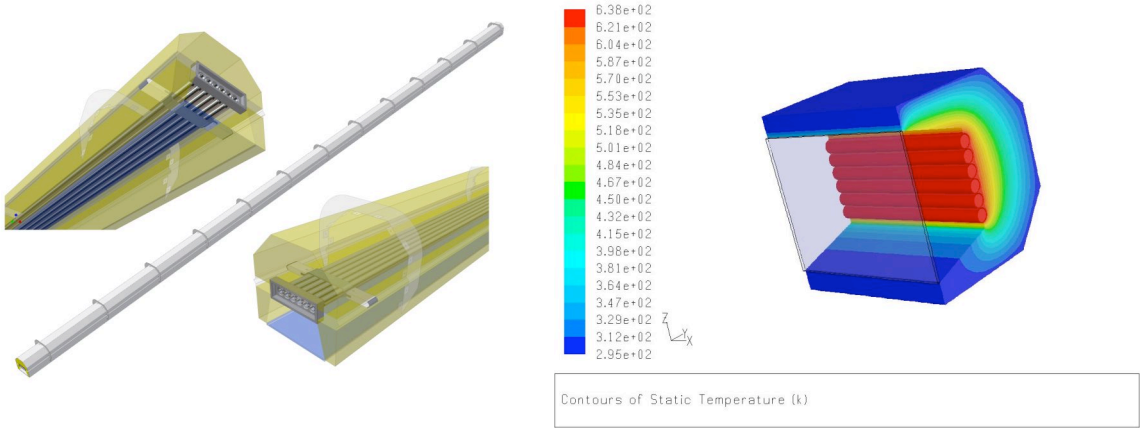

FIGURE 7: CAD IMAGE OF THE RECEIVER CONCEPT (LEFT). CONTOURS OF TEMPERATURE OBTAINED WITH A THERMO FLUID DYNAMICS SIMULATION OF THE RECEIVER (RIGHT). FIGURES TAKEN FROM [1].

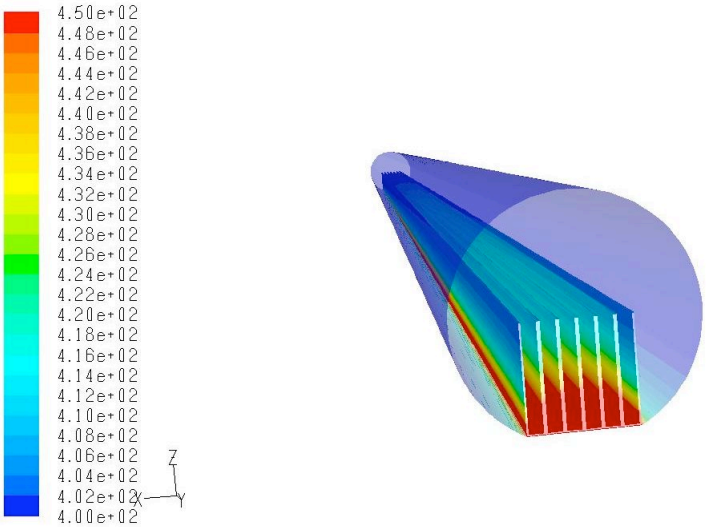

FIGURE 8: CFD SIMULATIONS OF STATIC TEMPERATURE CONTURS (SCALE IN K) FOR THE FINS OF THE MODEL 1 RECEIVER. AIR ENTERS THE DUCT AT 400 K. THE FLUID FLOW IS FROM BACK TO FORWARD.

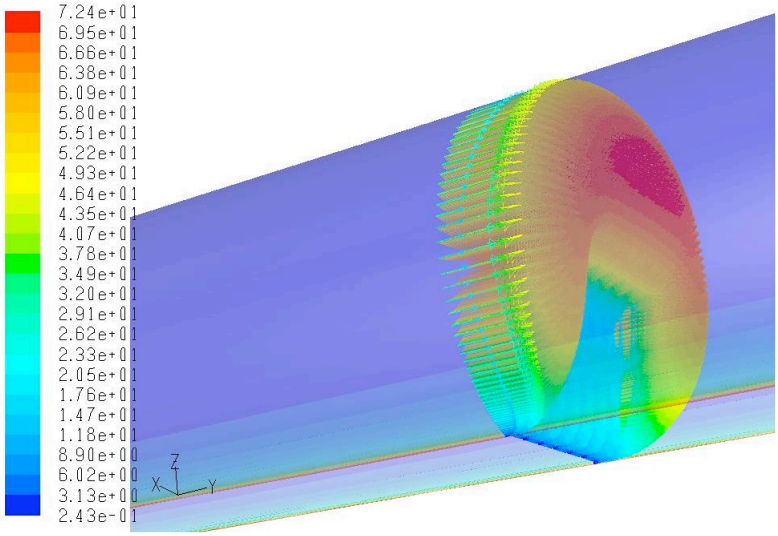

FIGURE 9: CFD SIMULATIONS OF MODEL 1 RECEIVER FLOW. THE FIGURE SHOWS THE VELOCITY VECTORS IN A SECTION OF THE RECEIVER DUCT. VECTORS ARE COLORED BY VELOCITY MAGNITUDE (THE SCALE IS IN m/s). AIR ENTERS THE DUCT AT 400 K. THE AIR FLOW SLOW DOWN IN THE FINS REGION IS NOTICEABLE.

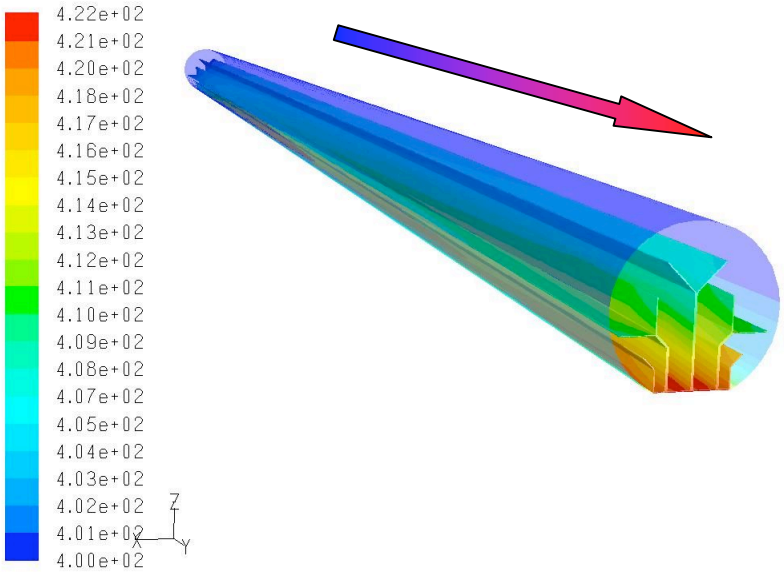

FIGURE 10: CFD SIMULATIONS OF STATIC TEMPERATURE CONTURS (SCALE IN K) FOR THE FINS OF THE MODEL 2 RECEIVER. AIR ENTERS THE DUCT AT 400 K. THE ARROW INDICATES THE FLUID FLOW DIRECTION.

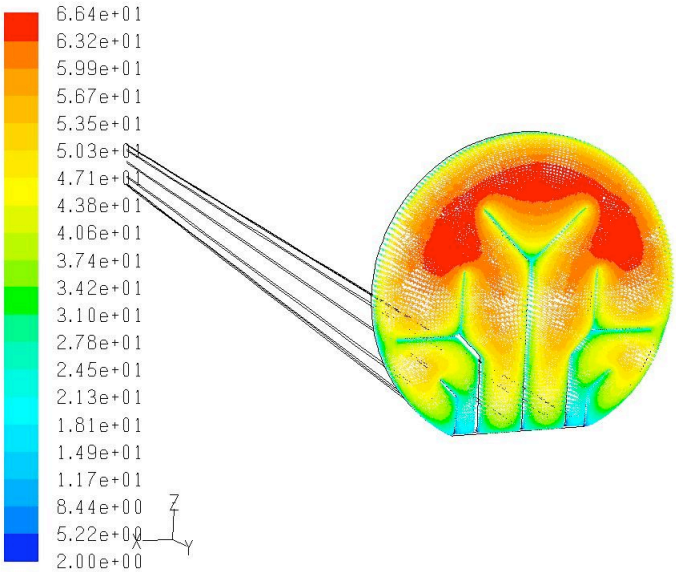

FIGURE 11: CFD SIMULATIONS OF MODEL 2 RECEIVER FLOW. THE FIGURE SHOWS THE VELOCITY VECTORS IN A SECTION OF THE RECEIVER DUCT. VECTORS ARE COLORED BY VELOCITY MAGNITUDE (THE SCALE IS IN m/s). AIR ENTERS THE DUCT AT 400 K.

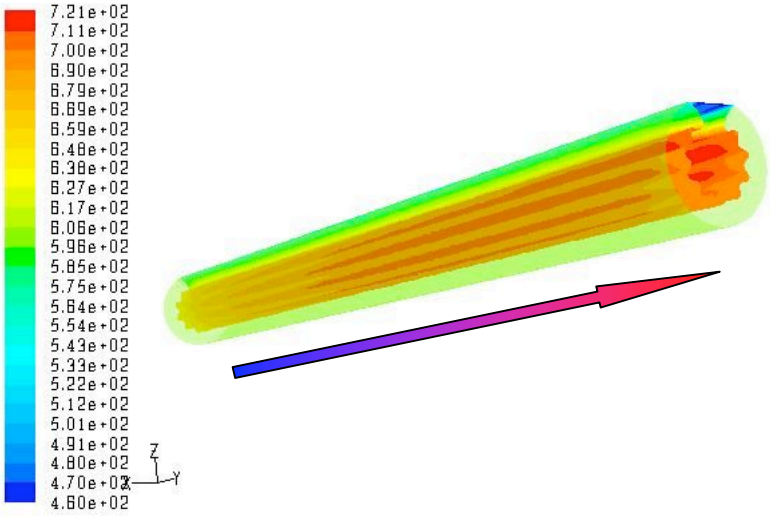

FIGURE 12: CFD SIMULATIONS OF STATIC TEMPERATURE CONTURS (SCALE IN K) FOR THE TARGET OF THE MODEL 5 CAVITY RECEIVER. AIR ENTERS THE DUCT AT 600 K. THE ARROW INDICATES THE FLUID FLOW DIRECTION.

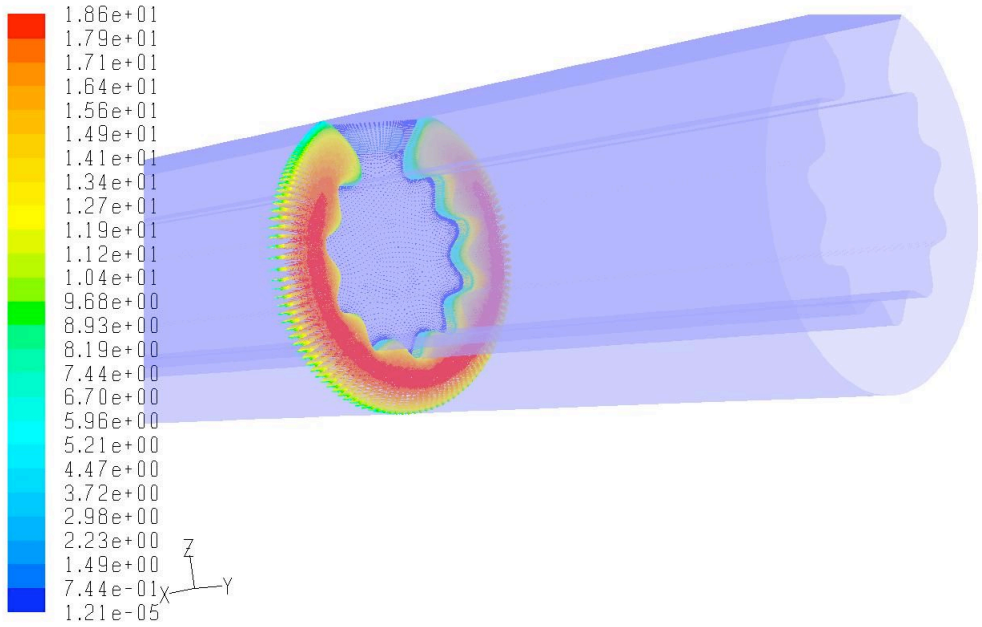

FIGURE 13: CFD SIMULATIONS OF MODEL 5 CAVITY RECEIVER FLOW. THE FIGURE SHOWS THE VELOCITY VECTORS IN A SECTION OF THE RECEIVER. AIR FLOWS IN A DUCT FORMED BY THE EXTERNAL CYLINDRICAL WALL AND THE INTERNAL WAVY TARGET. VECTORS ARE COLORED BY VELOCITY MAGNITUDE (THE SCALE IS IN m/s). AIR ENTERS THE DUCT AT 600 K.

receiver type	**working fluid**	**absolute press.** [bar]	**mass flow rate** [kg/s]	**pressure drop** [mbar]*	**temp. max target** [°C]	**temp. max glass** [°C]
mod-1	air	1.1	1.29	644	248*	n.a.
mod-2	air	2.0	1.27	647	250*	n.a.
mod-3	air	2.0	2.375	905	648	290
mod-4	air	2.0	2.375	241	677	163
mod-5	air	2.0	2.375	60	635	291
mod-5	air	8.0	2.375	20	620	277
mod-5	H_2O vapor	2.0	1.209	30	586	270
mod-8	air	1.1	2.375	23	623	377
mod-8	N_2	1.1	2.375	23	623	379

TABLE 1: SUMMARY OF MAIN RESULTS OBTAINED BY CFD SIMULATIONS FOR THE DIFFERENT TYPES OF RECEIVERS. PRESSURE DROPS ARE CALCULATED FOR A 250 M LONG RECEIVER AND THE TEMPERATURES LISTED ARE THOSE OBTAINED FOR THE STRONGEST THERMAL LOAD CONDITION. EXCEPTION IS MADE FOR THE VALUES WITH A STAR THAT ARE CALCULATED FOR COLD AIR AT INLET (INLET TEMPERATURE 400°C LOWER WITH RESPECT TO THE OTHERS). SCHEMATICS OF THE RECEIVER CROSS SECTIONS FOR THE MODELS LISTED CAN BE FOUND IN THE ANNEX A.

2 – SOLAR FLUX SIMULATIONS VIA MONTE CARLO METHOD (ETHZ)

A Monte Carlo ray tracing simulation of the SolAir solar concentrator has been established and implemented in Fortran 95. The Monte Carlo model takes into account the spatial extension of the sun, statistical tracking errors, random surface orientation errors of the mirrors, systematic mirror shape errors, due to a deformation of the system by its own weight, non-ideal reflectances, radiation losses through shading and end effects. The flux distribution and the 2-D concentration distribution in the focal plane, the flux distribution on the cavity absorber wall, and general system performance numbers have been calculated.

The obtained results have shown that the system is most sensitive to small deformations of the system structure caused to its own weight, as well as to surface slope errors of the mirrors, especially of the Primary Mirrors (PM). The ETFE-foil leads to a reduction of the incident solar radiation by about 7%.

By excluding all system-related imperfections, the theoretical maximum system performance has been determined, and the peak concentration ratio in the focal plane has been found to be 150 (see Figure 14). This result is in good agreement with the result for a comparable parabolic trough concentrator.

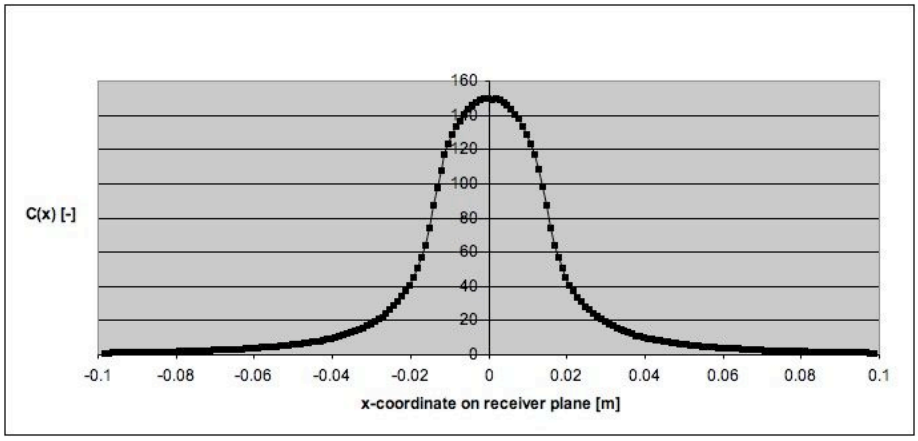

FIGURE 14: 2-D CONCENTRATION RATIO ON THE RECEIVER PLANE FOR THE IDEAL SYSTEM (AVERAGED ALONG THE OVERALL COLLECTOR LENGTH).

Using common literature values for the different system model parameters, a realistic system was simulated. Its peak concentration ratio amounts to 50 at solar noon and strongly decreases with increasing skew angles, due to crowing end losses and longer travel paths of the rays from the point of their reflection on the primary mirrors to the point of their absorption (Figure 15). The overall optical system efficiency for this configuration was found to be 55% (Figure 16).

Another research topic that has been explored is the cylindrical cavity receiver that is under investigation at SUPSI. Being this a promising receiver design, the optical cavity efficiency, i.e. the percentage of radiation incident on the focal plane that is intercepted and absorbed by the cavity, has been simulated via Monte Carlo Method. The results have shown that the optical cavity efficiency increases as the cavity wall absorptance increases. This occurs because captured rays are absorbed after a lower number of reflections reducing, as a consequence, their probability of escaping through the aperture. Figure 17 shows that optical cavity efficiency vary from 40% at an absorptance of 0.1 to about 75% at absorptance equal 0.9. In the same figure we notice also that the specularity of the cavity wall has negligible influence on the optical efficiency.
Another important effect of cavity surface absorptance is that, higher wall absorptances lead to higher non-uniformities of the flux distribution on the absorber surface, which is expected to be undesirable for the heat transfer to the heat transfer fluid (see Figure 3).

Moreover, there is a trade-off between the percentage of radiation intercepted by the cavity, and reflection losses through its aperture, and an optimum aperture size exists, which depends on the cavity wall absorptance. (see Figure 18).

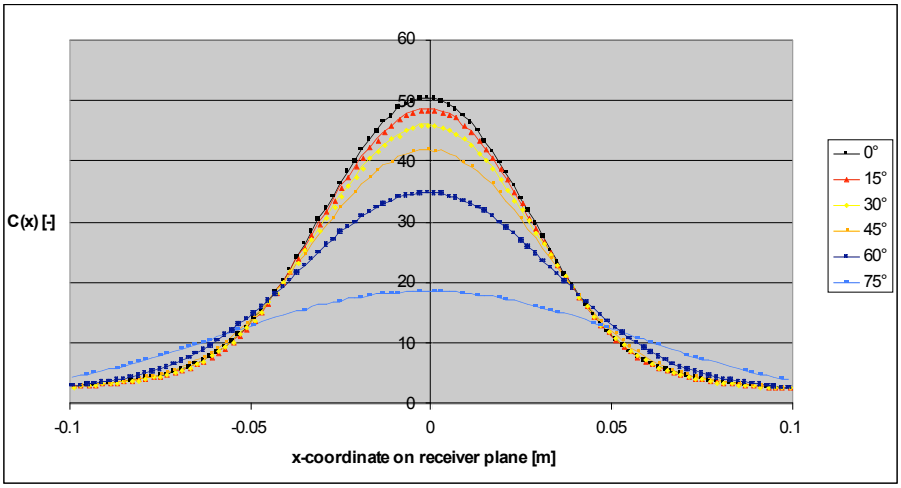

FIGURE 15: INFLUENCE OF DIFFERENT SKEW ANGLES ON FOCAL CONCENTRATION DISTRIBUTION OF A REALISTIC SYSTEM (AVERAGED ALONG THE OVERALL COLLECTOR LENGTH; SKEW ANGLES PARAMETRIC VALUES ARE REPORTED IN THE BOX ON THE RIGHT HAND SIDE).

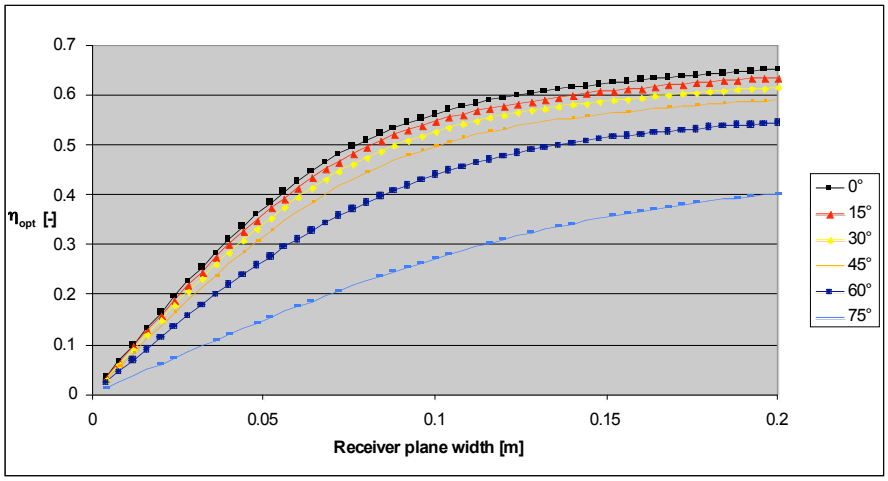

FIGURE 16: OPTICAL SYSTEM EFFICIENCY FOR A REALISTIC SYSTEM CONFIGURATION AT DIFFERENT SKEW ANGLES (SKEW ANGLES PARAMETRIC VALUES ARE REPORTED IN THE BOX ON THE RIGHT HAND SIDE).

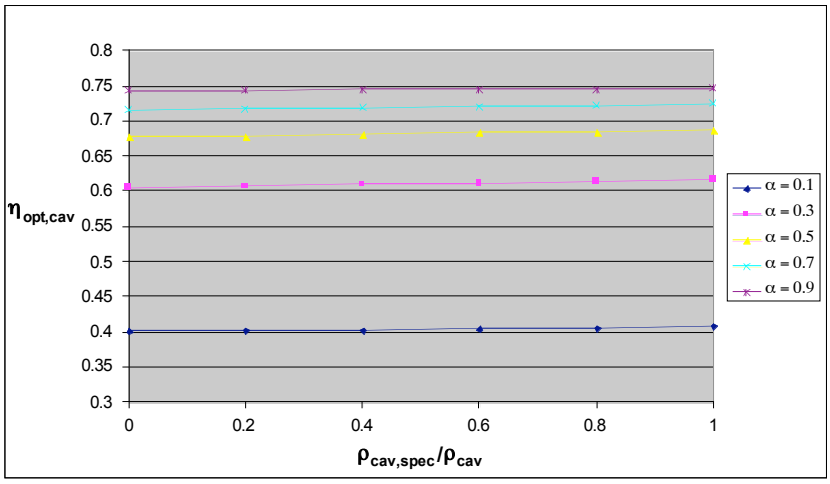

FIGURE 17: OPTICAL CAVITY EFFICIENCY PLOTTED VS THE RATIO OF TOTAL TO SPECULAR REFLECTANCE OF THE CAVITY WALLS. THE CURVES ARE PARAMETERIZED AS FUNCTIONS OF THE CAVITY SURFACE ABSORPTANCES (VALUES OF SURFACE ABSORPTANCE ARE REPORTED IN THE BOX ON THE RIGHT HAND SIDE).

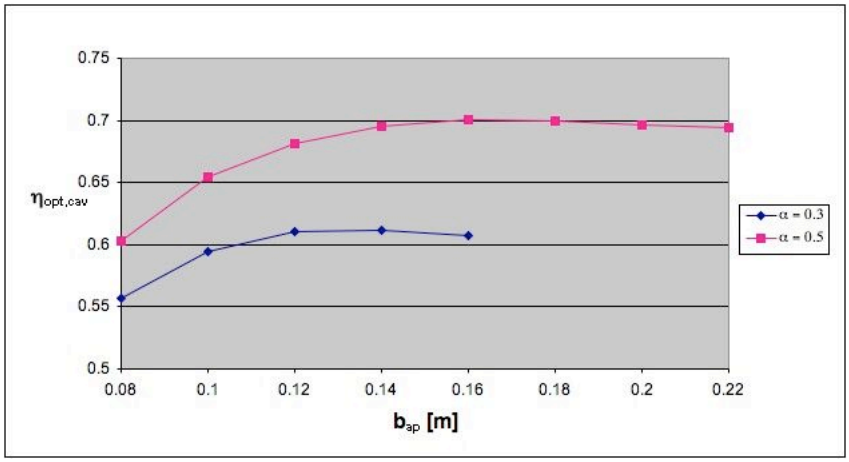

FIGURE 18: OPTICAL CAVITY EFFICIENCY AS FUNCTION OF THE CAVITY APERTURE WIDTH AT DIFFERENT CAVITY WALL ABSORPTANCES.

Modified system geometry, with a larger primary mirror aperture, has been also simulated and compared to the current prototype geometry. It shows significantly higher concentration ratios in the focal plane, but a lower optical efficiency, which may be caused by longer travel distances of the rays within the system (see FIGURE 19).

The simulations, of which the results have been briefly summarized, will be useful as a development tool for the concentrator and receiver optimization once that correct model parameters will be determined and a validation against measurements for the flux distribution in the focal plane of the real prototype system will be performed.

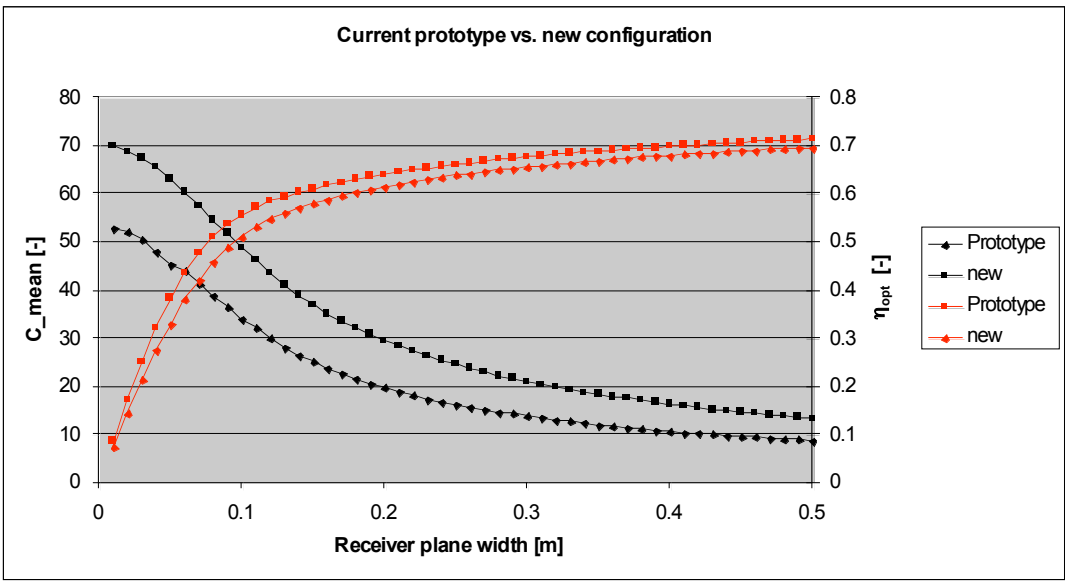

FIGURE 19: MEAN CONCENTRATION RATIO (BLACK) AND OPTICAL EFFICIENCY (RED) OF THE NEW CONFIGURATION COMPARED TO THE PROTOTYPE GEOMETRY (SIMULATIONS RESULTS).

3 – NEW PROTOTYPE CONSTRUCTION (AIRLIGHT)

3.1 – New collector prototype vs. first collector prototype

The new concentrator prototype is still based on the established Airlight concept of flexible pneumatic mirrors: perfectly cylindrical curved surface mirrors can be obtained by applying a few Pascal of over-pressure over a Mylar foil with a reflective aluminized coating on one side.

The design concept that allows to keep the primary mirror in tension and modify its shape as been kept. In fact, in the second prototype the cushion formed by the transparent ETFE foil on one side and a silicon fiberglass fabric on the other side contains two different volumes separated by the Mylar-reflective foil: the upper volume is enclosed by the ETFE and the primary mirrors whereas the lower one is realized by the primary mirrors and the silicon fabric. The application of different pressure values to the two volumes allows controlling accurately the primary mirrors shape. External computer controlled ventilators are used to inflate the cushion and manage the pressure differences.

The major differences between the first and second prototype can be seen comparing the two images of FIGURE 20 and FIGURE 21. Summarizing we can notice:

- the new receiver is located inside the ETFE cushion;
- the new collector has the primary mirror divided into two parts;
- the new collector makes use of secondary mirrors.

From the structural point of view several main components of the first prototype have been kept. From figures FIGURE 20 and FIGURE 21 we notice that longitudinal beams and rib beams are the same, as far as the metal supports for the structure and the collector tilting mechanism. The major changes have been done on the primary mirror that has been split in two allowing the insertion of a central metal frame that supports the receiver (see FIGURE 22 and FIGURE 23).

The fixing points for the ETFE membrane edges have been moved up and the technical issue of clamping the membranes edges has been solved using simple pre-cast and pre-stressed concrete frames having a rectangular shape. The external edges of the mylar primary mirrors have moved up too (see FIGURE 21 where these particular are been highlighted with a circle).

FIGURE 24 shows the door that has been designed to create a simple access way to the collector inner part. This entrance is at the end of a pressurized channel that is necessary for keeping stable the pressure inside the cushion and avoid mirrors movements during inspections and activities inside the collector.

With respect to the first prototype, the second one offers a series of advantages:

- receiver contained inside the ETFE cushion;
    - collector more compact and shorter travel distance of concentrated rays;
    - receiver not exposed to wind, i.e., less convective heat losses;
- solar radiation travels through the ETFE only once with a net recover of optical efficiency notwithstanding the use of secondary mirrors;
- secondary mirrors correct spherical aberration induced by the shape of primary ones;
- the internal part of the collector is easily accessible for control and maintenance;
- as proved by preliminary measurements, the concentration factor is greater than 50 suns.

In the following pages some photos of the working second prototype are shown (FIGURE 25 - FIGURE 26).

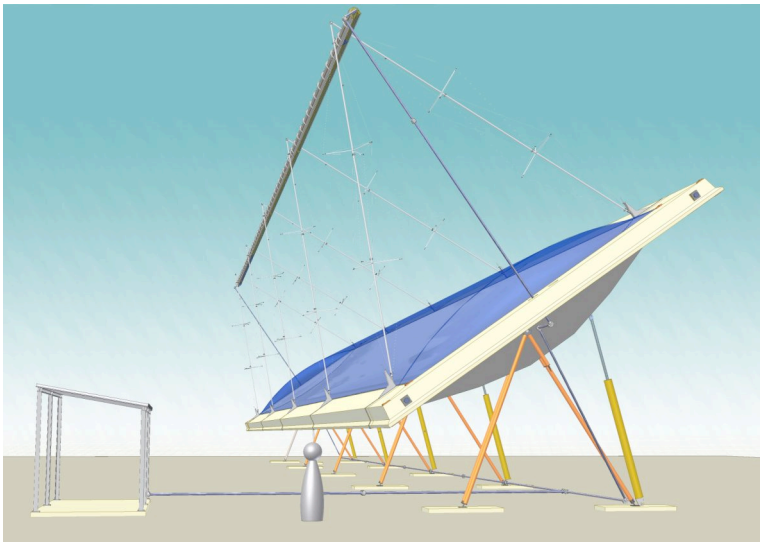

FIGURE 20: CAD IMAGE OF AIRLIGHT SOLAR COLLECTOR FIRST PROTOTYPE.

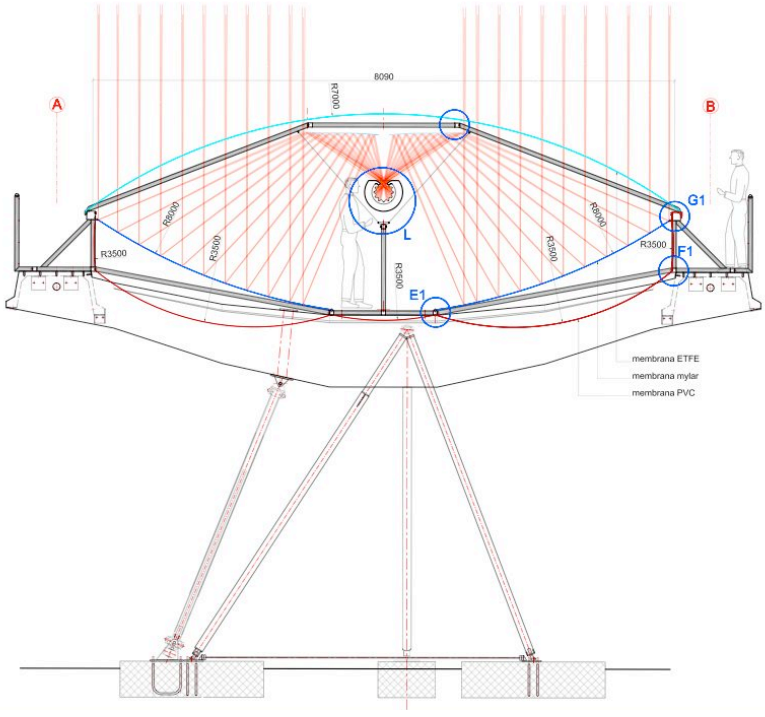

FIGURE 21: AIRLIGHT SOLAR COLLECTOR SECOND PROTOTYPE - CROSS SECTION OF THE TROUGH.

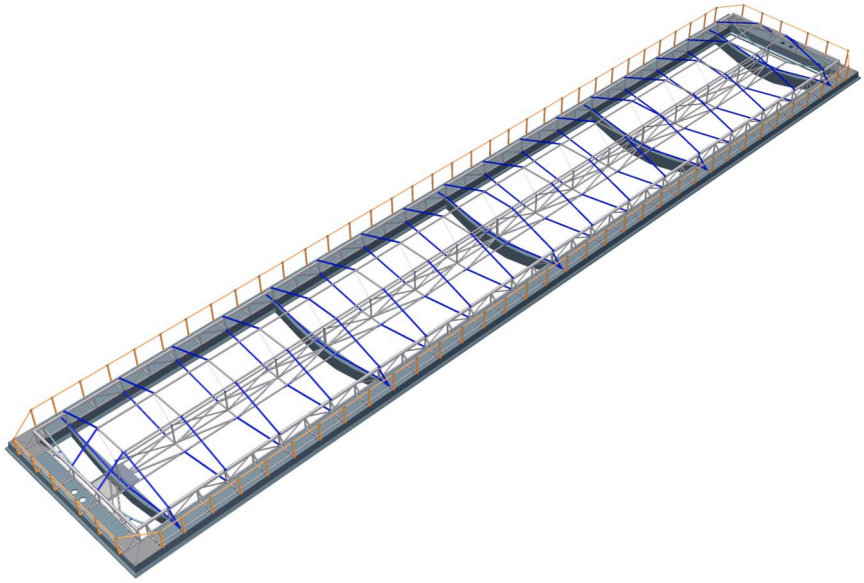

FIGURE 22: AIRLIGHT SOLAR COLLECTOR SECOND PROTOTYPE: STRUCTURE OVERVIEW.

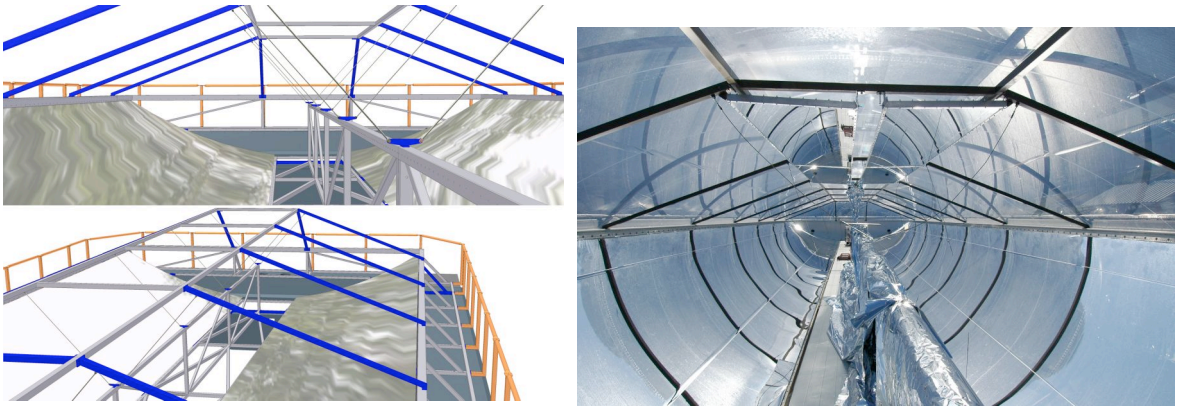

FIGURE 23: RENDERING (LEFT) AND REAL IMAGE (RIGHT) OF THE COLLECTOR INTERNAL PART.

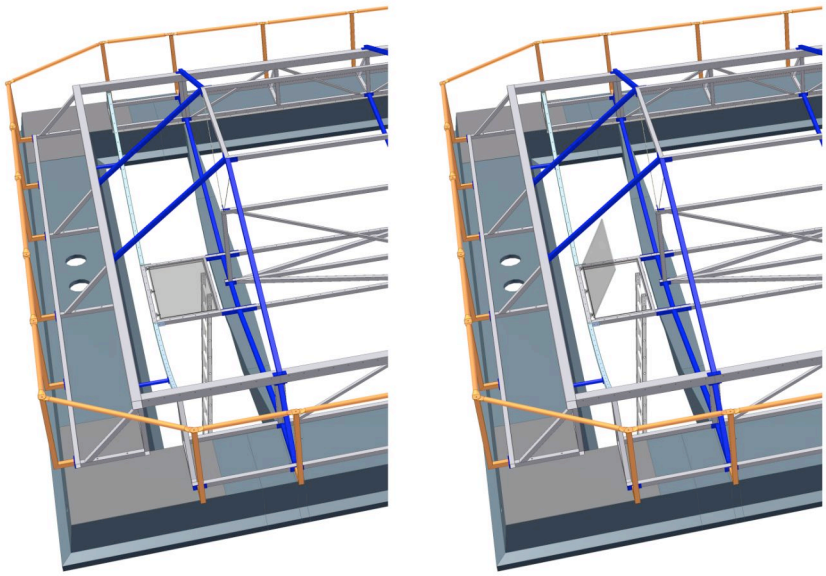

FIGURE 24: THIS IMAGE SHOWS THE PARTICULAR OF THE ENTRANCE DOOR TO THE INNER PART OF THE COLLECTOR PROTOTYPE. A SPECIAL PRESSURIZED ACCESS CHANNEL IS NECESSARY FOR KEEPING STABLE THE PRESSURE INSIDE THE CUSHION AND AVOID MIRRORS MOVEMENTS DURING INSPECTIONS AND ACTIVITIES INSIDE THE COLLECTOR.

FIGURE 25: ETFE FOIL DEPOSITION OVER THE SECOND PROTOTYPE.

FIGURE 26: SECOND PROTOTYPE: VIEW OF THE CONCRETE STRUCTURE. WE CAN NOTICE THE CURVED RIB BEAMS AND THE METAL SUPPORTS WITH THE HYDRAULIC TILTING SYSTEM.

FIGURE 27: VIEW OF THE NEW PROTOTYPE UP AND RUNNING.

3.2 – New collector concepts

A schematic image of the modified Airlight Collector concept can be seen in **FIGURE 28**. We can notice that it contains all the new prototype features. The concrete structure will be changed to include the novel tilting mechanism that will make use of the very rigid concrete frame. The novel shape of the rib beams can be seen in **FIGURE 29** where the new structure supports are also shown..

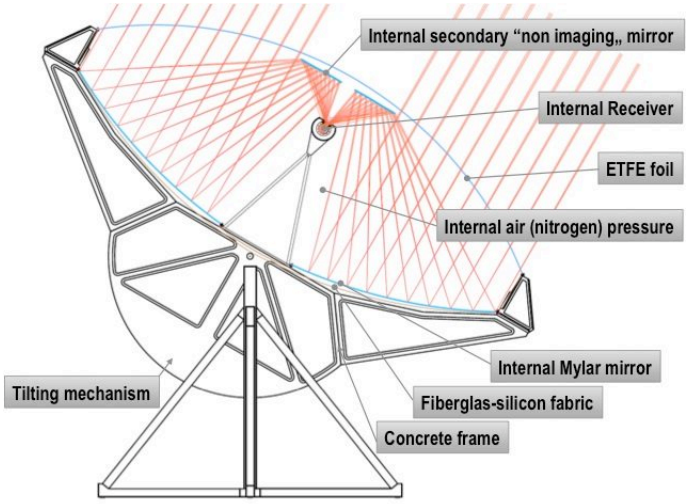

FIGURE 28: AIRLIGHT SOLAR COLLECTOR CONCEPT - CROSS SECTION OF THE TROUGH.

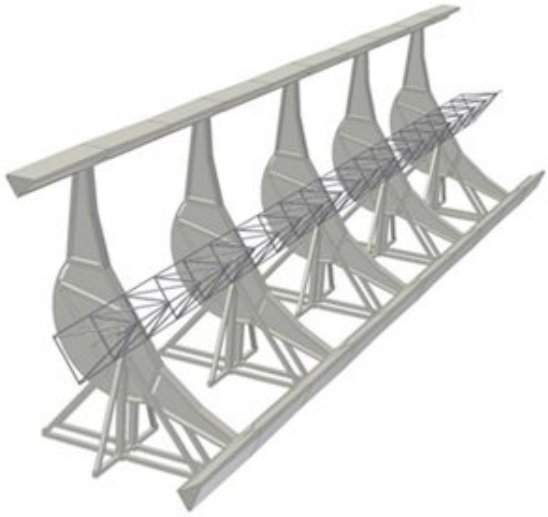

FIGURE 29: AIRLIGHT SOLAR COLLECTOR CONCEPT - CONCRETE FRAME OF THE TROUGH. THE SHAPE OF THE RIB BEAMS IS STUDIED TO INTEGRATE THE TILTING MECHANISM.

4 - Radiative Flux Measurements (ETHZ)

The AirLight prototype solar trough concentrator was optically characterized [9]. Radiative solar flux intensities were measured with a calibrated CCD camera by recording the image of the sun on a convection cooled Al_2O_3-coated Lambertian (a diffusely reflecting) plate positioned in the focal plane. After applying image offset and distortion corrections, the resulting grey values of the image were directly proportional to the incident radiative flux. The system has been calibrated by two absolute point radiometers, measuring simultaneously absolute flux on the Lambertian target.

4.1 COLLECTOR OPERATION PRINCIPLE

A primary mirror, made out of a reflective Mylar film of 0.4 mm thickness, measuring ca 8m across, and secondary mirrors of 2 m width, reflects and concentrates incoming solar radiation to the aperture of the absorbing receiver. The optical path is shown in **FIGURE 30**.

The concentrated solar radiation is absorbed by the heat exchanger surfaces of the receiver and transferred to the heat transporting medium.

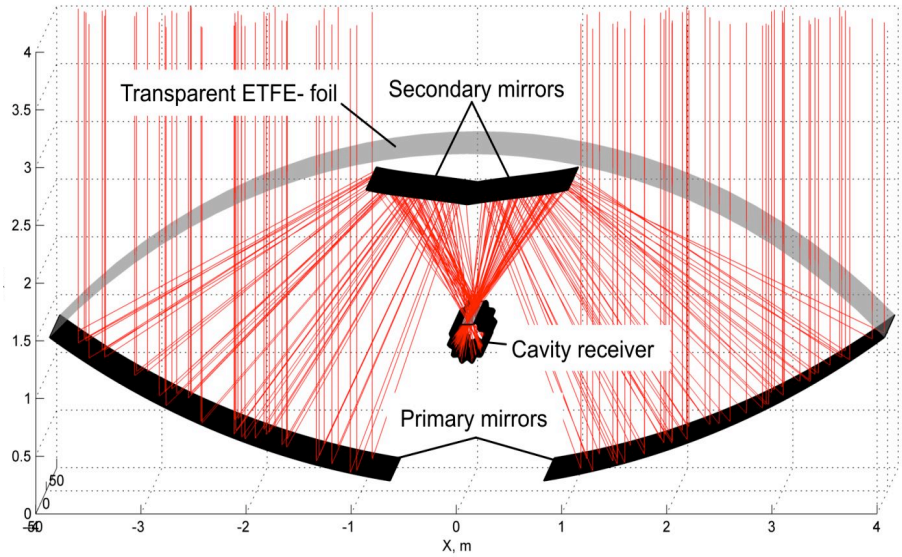

FIGURE 30: OPTICAL PATH FOR THE AIRLIGHT SECOND PROTOTYPE.

4.2 - Flux measurement

Exact knowledge of achieved concentration factor C, defined as the ratio of solar flux measured in the focal point divided by incident solar radiation and the spatial solar flux density distribution is important in the design process of efficient solar receivers.

4.3 - System description

The flux measurement system was designed and built for the geometrical properties and environmental conditions of the AirLight solar concentrator, based on the program T-flux and components used for measuring flux intensities and concentration in the solar simulator of ETH and in the solar furnace of PSI.

A Lambertian target is positioned in the focal plane of the solar concentrator and exposed to concentrated sunlight. Two calibrated heat flux gauges, attached onto the target's surface, continuously measure the absolute radiative flux in a circular area of 5 mm diameter. A progressive scan CCD

camera records the flux pattern imposed on the target. Direct solar irradiation is measured and recorded by an on-site sun tracking pyrheliometer. Data is recorded simultaneously by a central data acquisition system. Output parameters calculated by the flux measurement software is incident radiative power flux (in kW/m^2), peak and mean solar concentration ratio, and overall flux distribution over the receiver area. Integration of the radiative flux over a target area yields the incident solar power.

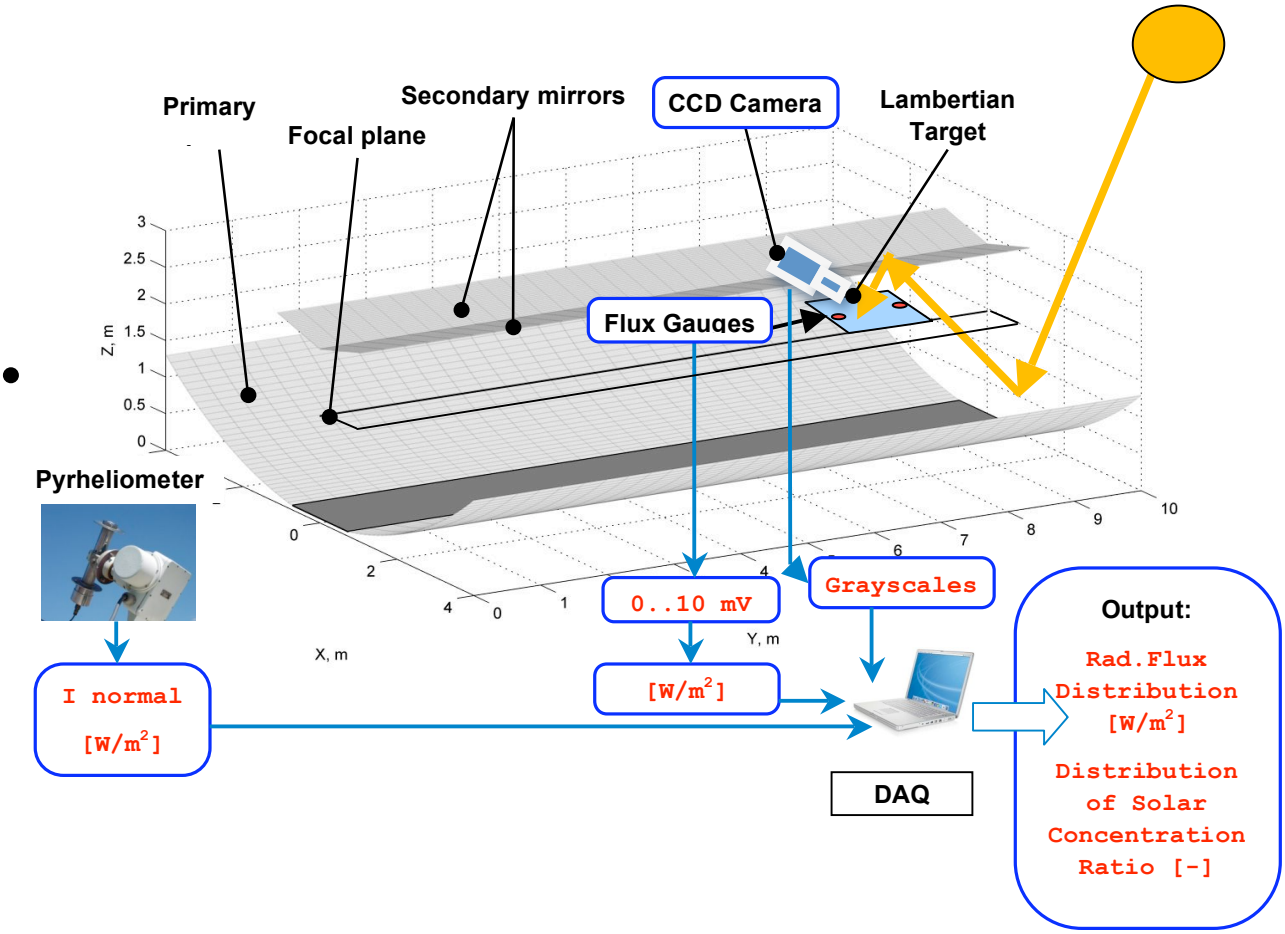

FIGURE 31: FLUX MEASUREMENT SYSTEM OVERVIEW.

4.3.1 - ACQUISITION AND DATA PROCESSING

Flux data acquisition and processing is performed according the following scheme:

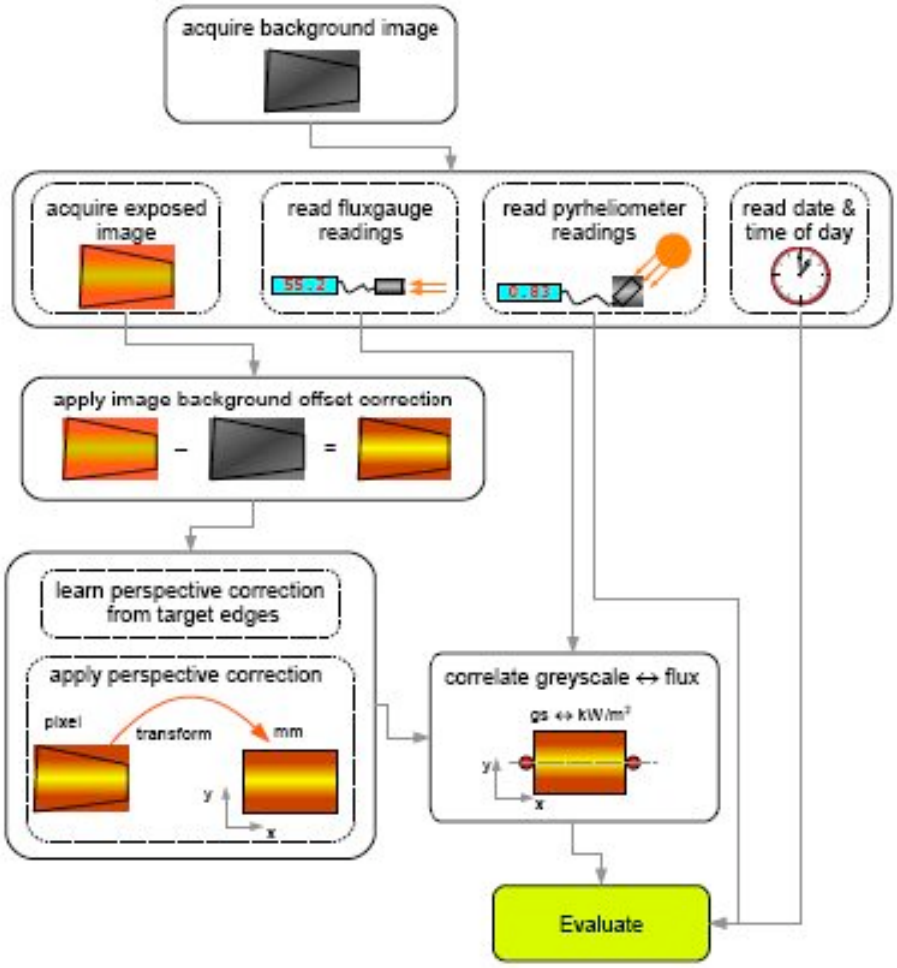

FIGURE 32: SCHEMATIC OF DATA ACQUISITION AND PROCESSING PROCEDURES.

4.4 System key components description

4.4.1 HEAT FLUX GAUGES

For calibration of camera recorded grey values to incident heat flux, two calibrated heat flux gauges are located in the target surface in a line parallel to the optical axis of the concentrating system in the field of view of the camera. During irradiation of the target, absolute flux data is collected. An image of a Vatell gauge is shown by **FIGURE 33**.

Manufacturer:	Vatell Corporation
Type:	Vatell TG 1000-0
Cooling:	water cooled, minimum flow rate: 1.5 l/min
Response Time:	to 95% of a step function > 1 sec
Calibration Accuracy:	+/-3%
Repeatability:	1%
Sensitivity:	Up to 2 mV/ (W/cm^2)
Transducer Coating:	high temperature black paint with flat spectral absorbance.
Emissivity:	0.94.
Output:	10mV maximum output. May be overdriven to 15mV
Calibration:	x-y calibration curve graph furnished with each transducer.

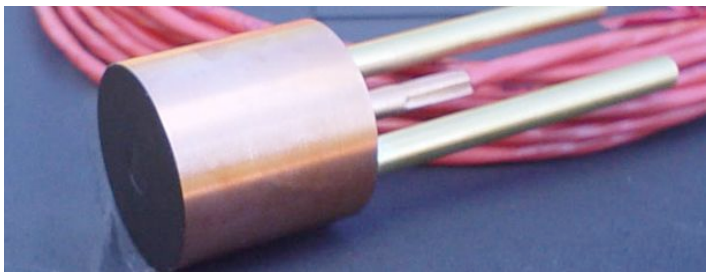

FIGURE 33: VATELL HEAT FLUX GAUGE.

4.4.2 PYRHELIOMETER

Pyrheliometer, Kip and Zonen, on tracker, installation on site, DAQ integrated in trough control system

4.4.3 LAMBERTIAN TARGET

The convective cooled target is a diffuse reflective screen, made out of ZrO2, positioned at the focal plane of the concentrator and within the field of view of the camera, is shown in **FIGURE 34**. For the calculation of the perspective view angle correction, the corners of the target are used as optical reference points.

Material:	ZrO_2
Dimensions:	410x610 mm, 20mm thickness
Cooling:	convection cooled
Mounting:	aluminum structure, two mounts for heat flux gauge

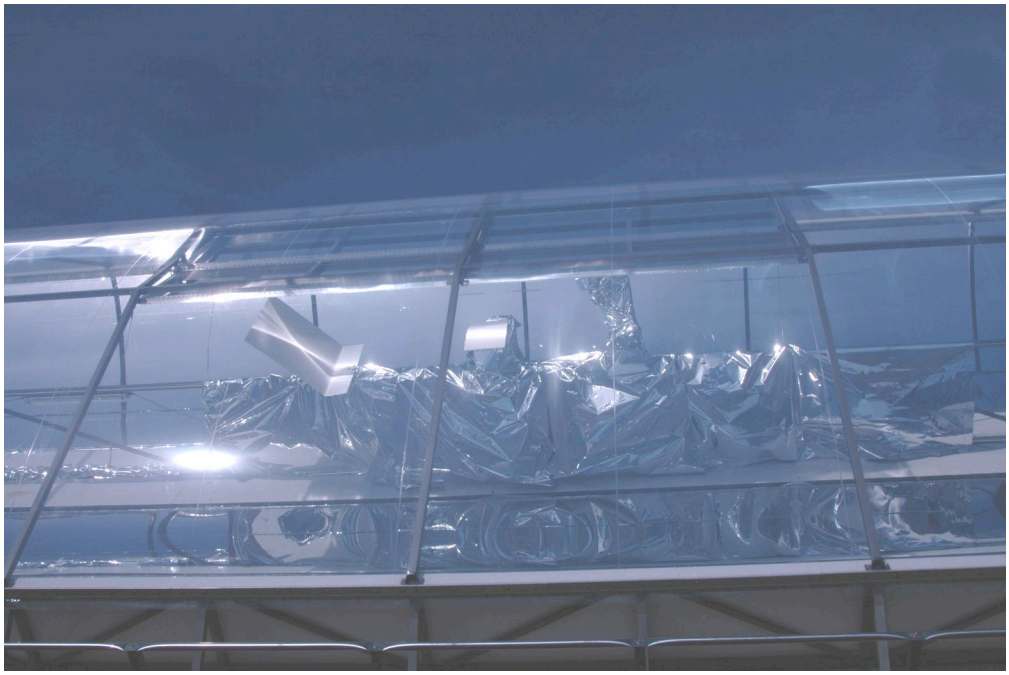

FIGURE 34: LAMBERTIAN TARGET DURING MEASUREMENT PROCEDURE.

4.4.4 CAMERA

The Basler progressive scan CCD camera 1392 x 1040 with a sigma auto focus lens and neutral density glass filters is mounted in optical axis close to secondary mirrors. Because of high thermal loads due to spillage of primary and secondary mirrors, the camera housing and optics are water cooled by means of attached heat exchanger plates and cooled by a closed water cooling circuit.

FIGURE 35: BASLER PROGRESSIVE SCAN CAMERA.

4.5 Results

4.5.1 BOUNDARY CONDITIONS

To achieve performance comparability under different solar irradiation intensities, flux measured is normalized by the incident radiation measured by the pyrheliometer, to give concentration factor C. Slight optical distortions on the primary mirror, coming from now corrected imperfections in the welding process, were avoided by choosing a representative on the primary mirror for the placement of the flux measurement system, shown in **FIGURE 36** and **FIGURE 37**. The target center was placed 18.545 m from the eastern end of the trough concentrator.

FIGURE 36: AREA OF FLUX CHARACTERIZATION.

4.5.2 FLUX MEASUREMENTS SEPTEMBER 25, 2008

The measurements took place on 25.September 2008. Direct normal insulation was steady between 800 W/m2 and 870 W/m^2 with no clouds. Three representative measurements with the last secondary mirror configuration are presented below.

All measurements were made under a constant differential pressure of 80 mbar between primary mirror membrane and outer shell. Increasing the differential pressure decreases the primary mirror radius and leads to shorter focal length. Differential pressure and target focal distance was slightly varied in order to collimate the two focal lines coming from each side of the mirror. The best conditions were found at 80 mbar and a target position between 350 388mm, where the flux measurements shown hereafter were performed.

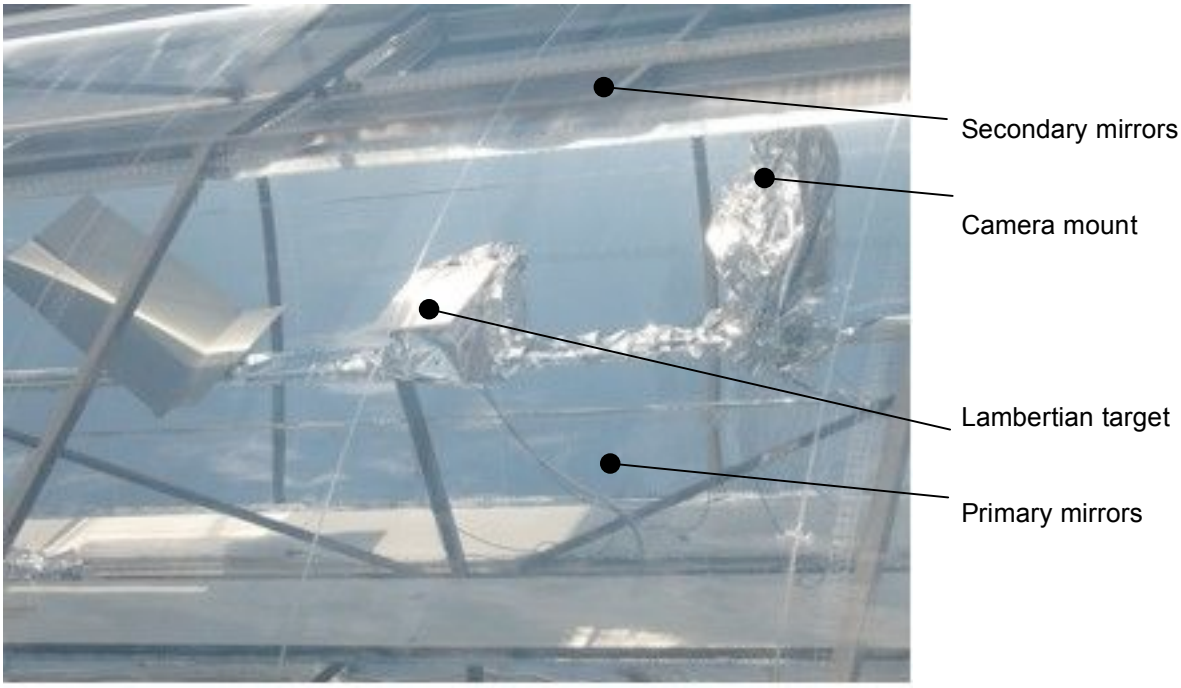

FIGURE 37: LAMBERTIAN TARGET AND CAMERA MOUNT.

4.5.3 FLUX MEASUREMENT DATA

FIGURE 38 shows the optical data after averaging and application of perspective correction.

A red line indicates the location of the cross section perpendicular to the optical axis of the concentrator trough where the concentration distribution is measured over the aperture and is shown in **FIGURE 39**.

The concentration average over the cross section in function of the aperture width is shown in **FIGURE 40** on the left side, and power integrated in function of aperture width, normalized to 1 m length of the focal line is shown on the right side.

CASE 1, FILENAME: 2008-09-25-11:56:17_TRNS_AVG_NO_0

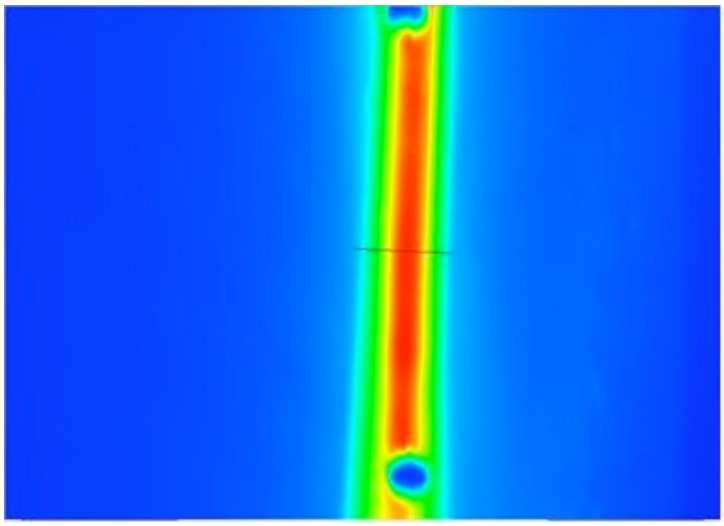

FIGURE 38: CALIBRATED CAMERA DATA CASE 1.

	Flux, kW/m^2	C Concentration
Average	23.34	28.50
Maximum	37.52	45.81

Time of measurement	11:56 LT
Solar Noon:	13.16 LT
Skew angle	-19.76°
Target position:	388mm
I solar	814 W/m2
C indicated radiometer Top	44.8
C indicated radiometer bottom:	44.2

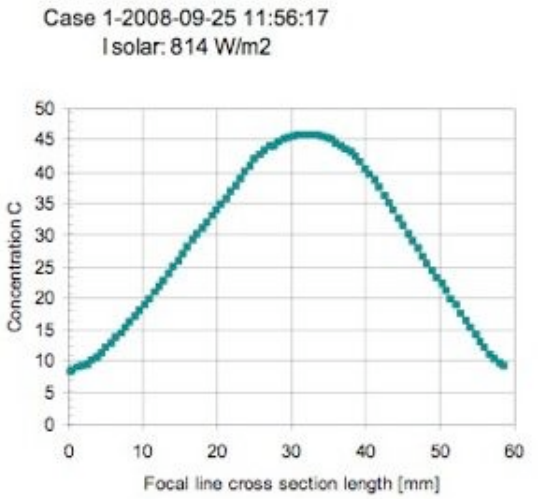

FIGURE 39: MEASURED CONCENTRATION DISTRIBUTION, CASE 1.

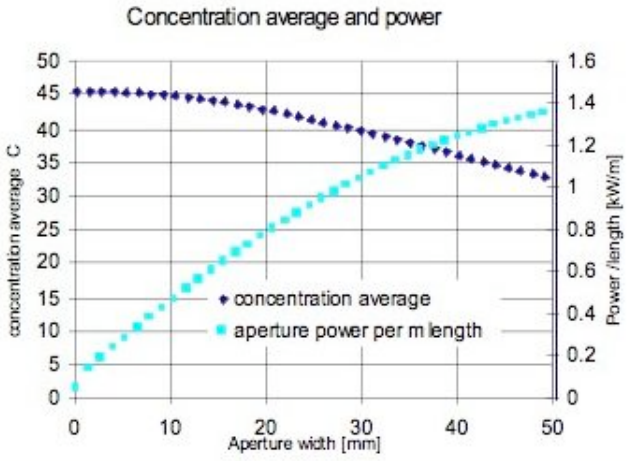

FIGURE 40: CONCENTRATION AND POWER, CASE 1.

CASE 2, FILENAME: 2008-09-25_131343_TRNS_AVG_NO_0

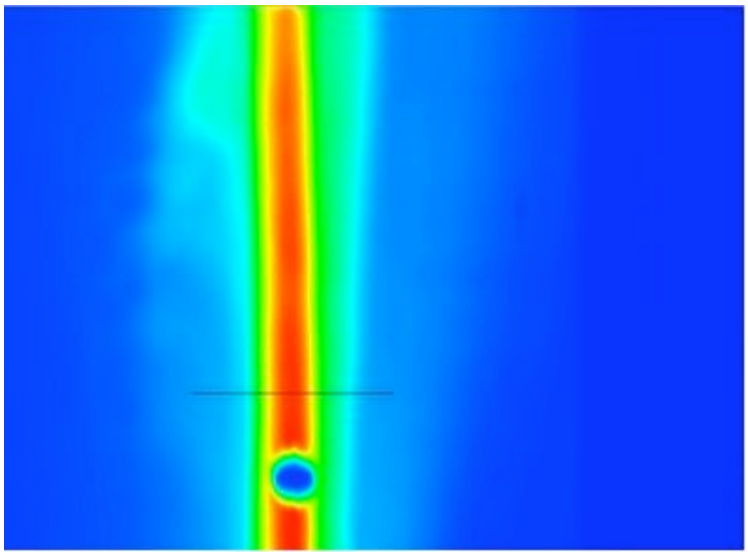

FIGURE 41: CALIBRATED CAMERA DATA CASE 2.

	Flux, kW/m^2	C Concentration
Average	17.38	19.98
Maximum	41.10	47.26

Time of measurement	13:14 LT
Solar Noon:	13.16 LT
Skew angle	-0.4°
Target position:	385mm
I solar	869 W/m^2
C indicated radiometer Top	39.7
C indicated radiometer bottom:	47

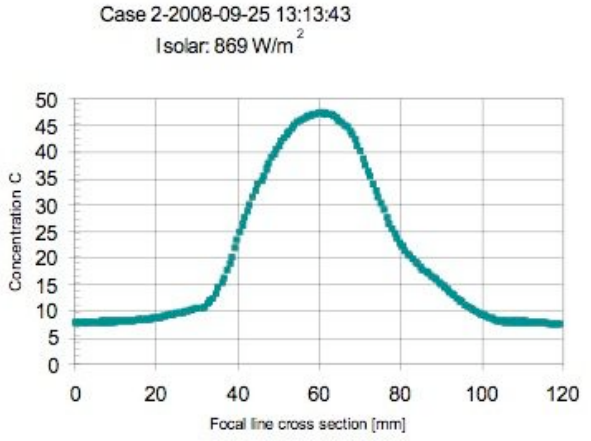

FIGURE 42: MEASURED CONCENTRATION DISTRIBUTION, CASE 2.

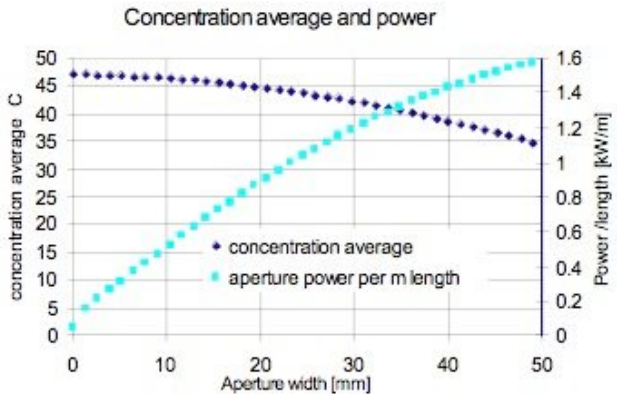

FIGURE 43: CONCENTRATION AND POWER, CASE 2.

CASE 3 FILENAME: 2008-09-25-13:49:40_TRNS_AVG_NO_0

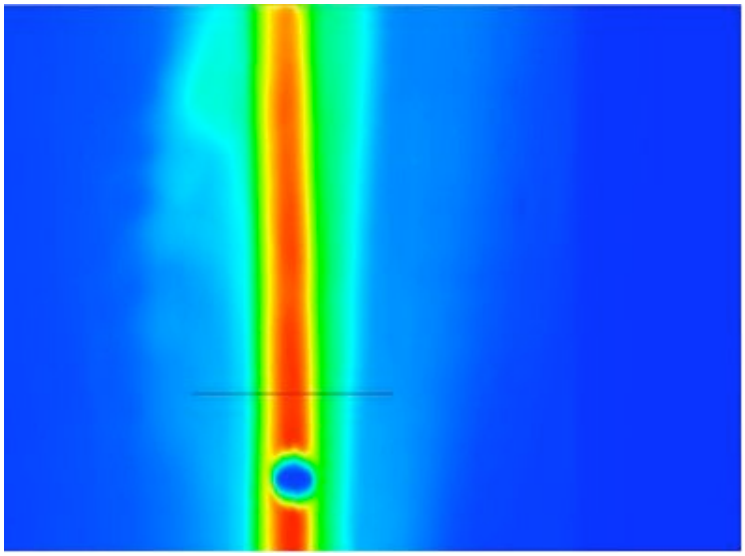

FIGURE 44: CALIBRATED CAMERA DATA CASE 3.

	Flux, kW/m^2	C Concentration
Average	16.89	19.63
Maximum	47.79	55.56

Time of measurement	11:56 LT
Solar Noon:	13.49 LT
Skew angle	8.64°
Target position:	350.5mm
I solar	860 W/m2
C indicated radiometer Top	44
C indicated radiometer bottom:	55

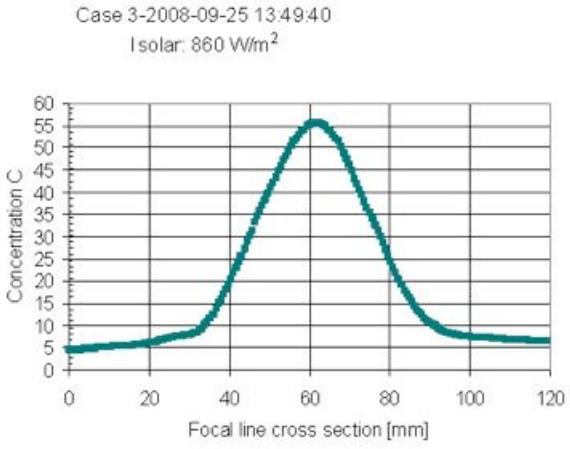

FIGURE 45: MEASURED CONCENTRATION DISTRIBUTION, CASE 3.

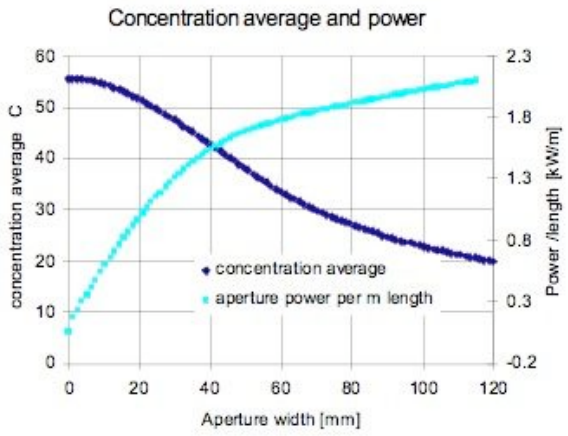

FIGURE 46: CONCENTRATION AND POWER, CASE 3.

4.5.4. IDEALIZED SECONDARY MIRROR:

As the curved shape secondary mirrors, required to correct the spherical aberration of the system, were not available, a set of flat secondary mirrors, made out of reflective Mylar film stretched over a frame have been used during the measurements. With these non ideal secondary mirrors, peak concentrations in the range of 45-65 were achieved.

A comparison between measured concentration and a Monte Carlo simulation of concentration using ideal secondary mirrors is shown in **FIGURE 47**.

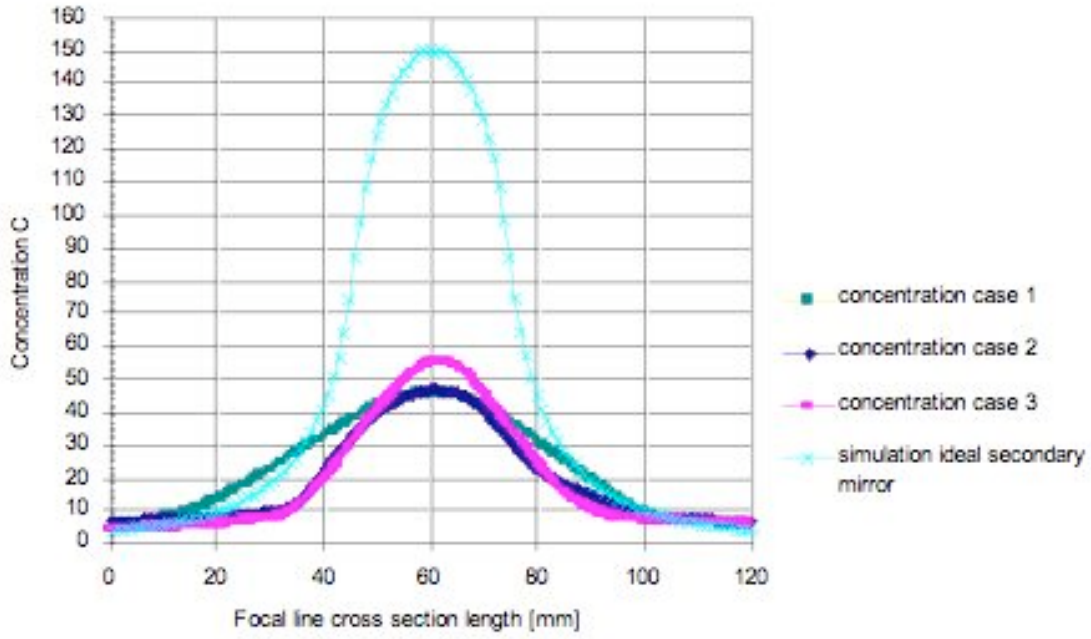

FIGURE 47: COMPARISON WITH SIMULATION OF IDEAL SECONDARY MIRROR.

Collaboration nationale

The project is a scientific collaboration among Airlight, SUPSI and ETHZ. For the SUPSI the collaboration is with the Institute for Computer Integrated Manufacturing for Sustainable Development of the Innovative Technologies Department. For the ETHZ the collaboration is with the Institute of Energy Technology of the Mechanical and Process Engineering Department.

Collaboration internationale

Not applicable.

Évaluation du travail effectué et de ses perspectives pour le reste de l'année.

The present project was successfully completed. The work performed by the Partners brought to the design, realization and optical characterization of the second ALE Airlight collector prototype.

ALE Airlight completed successfully the second prototype construction, which involved a major change of the mirrors concept, by splitting the primary mirror in two, adding secondary mirrors, and inserting the receiver inside the ETFE cushion. A novel and more efficient concept for the collector tilting mechanism has been also defined.

ETHZ modeled the optical characterization of the collector mirrors system via Monte Carlo simulations. Further work was done for the optical characterization of a cylindrical cavity receiver.

SUSPI performed the receiver study and design by using thermo-fluid dynamics simulations. Several different solutions of receiver have been explored and evaluated in agreement with the new configuration of the collector prototype and the new working fluids adopted.

ALE Airlight and ETHZ performed an intensive measurements campaign on the prototype. The gathered data were used to characterize the novel collector by defining its real performances, and to carry out the tuning of the computer simulations models set up and used by ETHZ and SUPSI.

A more detailed summary of main project conclusions is reported in the following paragraph.

CONCLUSIONS

Receiver

The receiver for the Airlight collector has to offer a favorable combination of economical and technical factors. It must effectively transform concentrated radiative energy into working fluid thermal energy and it has to be cheap. Furthermore, because of the very large volumes of air that will circulate into Airlight receivers, pressure losses into these ducts represent another critical issue that directly hits the solar plant global efficiency. Therefore, to keep low the pressure losses, the flow speed into the receivers has to be maintained low. This means large ducts cross sections but also large target surfaces to preserve an effective convective heat exchange.

The study on the Airlight Collector receiver, carried out taking these factors into account, brought to the conclusion that the one that matches at best all the above design constraints is Model 8 (see Annex A). This receiver has a target with a wide and smooth surface. The simulations showed that the models with a corrugated target surface do not bring very significant advantages. Furthermore, Monte Carlo simulations showed that the corrugated shape of the target produces some undesirable hot spots i.e., regions where the radiative flux is concentrated. This problem should be less relevant on targets with smooth surfaces.

From the fabrication point of view, for an assigned target duct mean diameter, receivers with smooth targets are also cheaper than corrugated ones both because of the lower quantity of metal per meter of length and of the lower manufacture costs.

A further optimization of the receiver design is expected to come from a tight coupling of the thermo fluid dynamics simulations (CFD) with the solar flux simulations via Monte Carlo method. The latter, applied to the new collector and receiver geometries will give more accurate concentrated solar flux

distribution on the receiver target. These data will be used as boundary conditions for the new CFD simulations.

Solar Flux Simulations via Monte Carlo Method

A simulation was established that produces reasonable results for the focal flux distribution, as was found by a comparison with the result from literature for a parabolic trough concentrator with approximately the same rim angle. The simulation allows for the adjustment and investigation of a broad range of system parameters. The flux distribution and the 2-D concentration distribution in the focal plane, the flux distribution on the cavity absorber wall, and general system performance numbers can be calculated.

First results show that the system is most sensitive to small deformations of the system structure caused to its own weight, as well as to surface slope errors of the mirrors, especially of the primary mirrors. The ETFE-foil leads to a reduction of the incident solar radiation by about 7%.

By excluding all system-related imperfections, the theoretical maximum system performance was determined, and the peak concentration ratio in the focal plane was found to be 150. This result is in good agreement with the result for a comparable parabolic trough concentrator.

Using common literature values for the different system model parameters, a realistic system was simulated. Its peak concentration ratio amounts to 50 at solar noon and strongly decreases with increasing skew angles, due to crowing end losses and longer travel paths of the rays from the point of their reflection on the primary mirrors to the point of their absorption. The (overall) optical system efficiency for this configuration was found to be 55%.

The optical cavity efficiency increases as the wall absorptance increases, and its values vary from 40% at wall cavity absorbance of 0.1 to 75% at a wall cavity absorbance of 0.9. Generally, higher wall absorptances lead to higher non-uniformities of the flux distribution on the absorber surface, which is expected to be undesirable for the heat transfer to the heat transfer fluid.

Moreover, there is a trade-off between the percentage of radiation intercepted by the cavity, and reflection losses through its aperture, and an optimum aperture size exists, which depends on the cavity wall absorptance. The optical cavity efficiency was found to be largely independent of the specularity of its surface.

Radiative Flux Measurements

Direct radiative flux measurements enable the determination of the optical system performance. Calibration is accomplished by absolute radiometers coupled to the flux- mapping system. The total solar power input to the receiver is found by numerical integration of the power flux distribution over the receiver's aperture area. The distribution of the solar concentration ratio and power input are important parameters for dimensioning the receiver aperture. The higher the solar concentration ratio, the smaller the receiver's aperture, minimizing the radiative losses and, consequently, increasing the energy conversion efficiency. A peak solar concentration ratio of 55 was measured, which compares well to existing systems, e.g. EuroThrough. Using Fig. 18, an average solar concentration ratio of C=30 was measured for a receiver aperture of 70 mm. Power collected within 1 m of length and 70 mm aperture was 1.8 kW.

The system is sensitive to slight variations in radius of curvature of the primary mirrors. While the location of the focal plane can be influenced easily by variation of membrane air pressure, great care must be taken to keep the radius of curvature constant over the length of the mirror module in the manufacturing process. Flux mapping the full concentrator length will be able to track local variations over the full length of the concentrator and will lead to a better understanding of the system performance.

Références

[1] Barbato, M.C. Haueter, Ph., Coray, P., Steinfeld, A., Pedretti, A., "Solair Project Annual Report", December 2007.

[2] Bader, R., "Monte Carlo Simulations of a Novel Circular Trough Solar Collector", Master Thesis, Swiss Federal Institute of Technology Zurich, June, 2008.

[3] Lior, N., "Thermal Theory and Modeling of Solar Collectors" in *Solar Collectors, Energy Storage, and Materials* edited by F. de Winter, MIT, pp. 99-182, 1990.

[4] Boyd D.A., Gajewski R., Swift R., "A Cylindrical Blackbody Solar Energy Receiver", *Solar Energy*, Vol. 18, pp. 395-401, 1976.

[5] Barra O.A., "*La conversione fototermica dell'energia solare*", Etas Libri, 1981.

[6] Barra O.A., "The Parabolic Trough Plant Using Black Body Receivers: Experimental and Theoretical Analyses", *Solar Energy*, Vol. 38, No. 2, pp. 163-171, 1982.

[7] Shih T.-H., Liou W.W., Shabbir A., Yang Z., Zhu J., "A new k-epsilon eddy viscosity model for high Reynolds number turbulent flows", *Computers and Fluids*, Vol.24, No. 3, pp. 227-238, March 1995.

[8] Kader, B.A., "Temperature and Concentration Profiles In Fully Turbulent. Boundary Layers", *International Journal of Heat and Mass Transfer*, Vol. 24, No. 9, pp. 1541-1544, 1981.

[9] Haueter, Ph., Bader, R., Steinfeld, A., "Radiative Flux Measurement and Monte Carlo Ray-Tracing Simulation and Validation", ETHZ – Technical Report, November 2008.

Annexes

- Annex A: CAD schematics of receiver types developed at SUPSI.
- Annex B: Monte Carlo ray-tracing simulation validation.
- Annex C: Measured geometry data.
- Annex D: Extracted geometry data.